MAJIS VIS-NIR channel: Performances of the Spare Model Focal Plane Unit

Nuno Pereira[a], Miriam E. Cisneros-González[a,b], David Bolsée[a], Lionel Van Laeken[a], Ann C. Vandaele[a], Samuel Gissot[c], Yves Langevin[d], Paolo Haffoud[d], and François Poulet[d]

[a]Royal Belgian Institute for Space Aeronomy (BIRA), Av. Circulaire, 1180 Brussels, Belgium
[b]Institute of Condensed Matter and Nanosciences, Université catholique de Louvain, Place de l'Université, 1348 Ottignies-Louvain-la-Neuve, Belgium
[c]Royal Observatory of Belgium (ROB), Av. Circulaire, 1180 Brussels, Belgium
[d]Institut d'Astrophysique Spatiale (IAS), Rue Jean-Dominique Cassini, 91440 Orsay, France

ABSTRACT

MAJIS (Moons And Jupiter Imaging Spectrometer) is the visible and infrared imaging spectrometer of the ESA L-Class mission JUICE (JUpiter Icy moons Explorer). MAJIS plays a major role for achieving the JUICE main scientific objectives, which include the compositional study of the Galilean moons, their past and present activity, and its relation with observed surface features. It will also study the composition, structure, chemistry and dynamics of the Jovian atmosphere. MAJIS is composed of two spectral channels: the VIS-NIR (0.5µm-2.35µm), and the IR (2.25µm-5.54µm). Both channels are equipped with a Focal Plane Unit (FPU) mainly including a Teledyne H1RG Focal Plan Array (FPA), one Focal Plane electronics (FPE) and one filter. A dedicated facility was developed at the Royal Belgian Institute for Space Aeronomy (BIRA-IASB) for the characterization of the Flight (FM) and Spare (SM) models of the MAJIS VIS-NIR FPU. The radiometric capabilities of the facility include: (1) the tuning of the monochromatic flux provided to the detector over a four-decade range of intensity, (2) optical configurations for dark conditions, uniform light beam or convergent light beam with the same focal ratio as MAJIS, and (3) relative and absolute radiometric scales at the FPA plane. This work describes the radiometric characterization campaign of the MAJIS VIS-NIR SM FPU and the respective data analysis methods used to derive some of the detector key parameters such as the gain, the dark current, the linearity, the full-well capacity and the operability. A comparison with the performances of the FM VIS-NIR FPU is also provided.

Keywords: MAJIS, JUICE, VIS-NIR channel, H1RG

1. INTRODUCTION

The next ESA L-Class mission to the Jovian System is the Jupiter Icy Moons Explorer (JUICE), which will launch in 2023 and arrive at Jupiter in 2030.[1] Ten state-of-the-art scientific instruments, divided in three different packages, compose the JUICE payload. The Moons and Jupiter Imaging Spectrometer (MAJIS) is a key scientific instrument in the remote sensing package. MAJIS aims to study the composition and physical properties of the surfaces of the Galilean satellites, characterize their exospheres, study the atmosphere of Jupiter at different levels (including auroras, magnetic footprints and hotspots), characterize the whole Jovian system (including ring system, dust and small inner moons), and monitor particular aspects of the satellites (including Io and Europa torii and Io's volcanic activity).[2]

MAJIS is a hyperspectral imager spectrometer providing visible (VIS) and infrared (IR) information through two channels: VIS-NIR (0.5 µm - 2.35 µm), and IR (2.25 µm - 5.54 µm). To verify and validate the performances of the MAJIS detectors within the in-flight operation, they were radiometrically characterized by reproducing high-vacuum and cryogenic conditions in a safe and controlled environment, before being integrated on the

Further author information: (Send correspondence to N.P.)
N.P.: E-mail: nuno.pereira@aeronomie.be, Telephone: +32 (0)2 373 03 51, B.RCLab: https://brclab.aeronomie.be/
M.C.: E-mail: miriam.cisneros@aeronomie.be, Telephone: +32 (0)2 373 03 50

Space Telescopes and Instrumentation 2022: Optical, Infrared, and Millimeter Wave, edited by Laura E. Coyle, Shuji Matsuura, Marshall D. Perrin, Proc. of SPIE Vol. 12180, 121803I · © 2022 SPIE · 0277-786X · doi: 10.1117/12.2642675

spacecraft. The Royal Belgian Institute for Space Aeronomy (BIRA-IASB) was in charge of the characterization of the Flight (FM) and Spare (SM) Models of the MAJIS VIS-NIR detectors, with the technical and scientific support of the *Institut d'Astrophysique Spatiale* (IAS), the lead institute of the MAJIS instrument.[3]

At instrument level, the MAJIS VIS-NIR detector is integrated in a mechanical package, known as the Focal Plane Unit (FPU), that guarantees the nominal cleanliness, thermalization, straylight rejection and optical alignment of its internal components (Fig. 1).[4] The FPU is composed by:

- **Focal Plane Array (FPA)**, which consists of a 1024×1024 pix^2 H1RG HgCdTe Teledyne detector array.
- **Focal Plane Electronics (FPE)**, composed by the SIDECAR/ASIC module to read out the FPA.
- **Linear Variable Filter (LVF)**, a cut-off high pass VIS-NIR filter to effectively reject high diffraction orders from the VIS-NIR grating, and filter the thermal background signal from the spectrometer itself and other forms of straylight.
- **Zero order mirror**, to suppress the zero order light rejected by the VIS-NIR grating.
- **Focal Plane Flex (FPF)**, the flex cable interface between the FPA and the FPE.
- **Focal Plane Assembly (FPAssy)**, the thermo-mechanical housing of the FPU.
- **FPE-OH**, which consists of the internal harness to link the FPE to the Optical Head (OH).

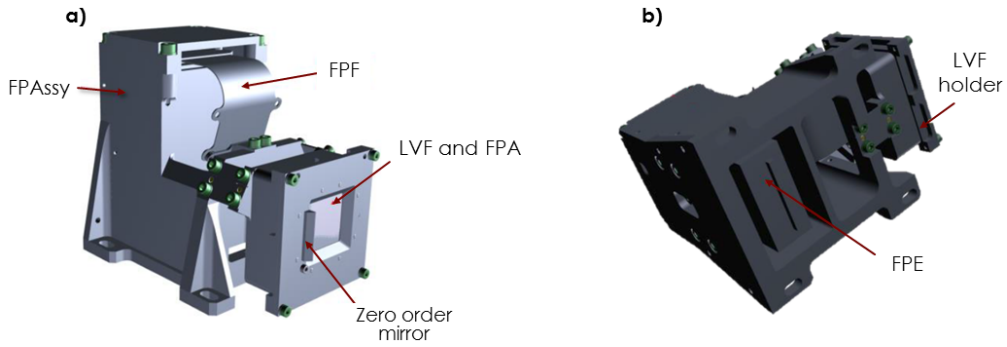

Figure 1. General views of the MAJIS VIS-NIR FPU: a) Frontal-top view, b) Rear-bottom view.[4]

The characterization campaign for the MAJIS FM VIS-NIR took place in 2020 and for the SM detector in 2021. During the FM campaign, the FPU was characterized with and without the LVF.[3] For the SM campaign, the SM detector was characterized only in its final configuration, i.e, with the FPU equipped with the LVF, to mitigate the planning constraints. The characterization of the performances of the SM detector consists in measuring the parameters listed in Fig. 2. Note that each of them requires different temperatures and illumination conditions. In addition, data acquisition can be performed at different integration times and readout modes.

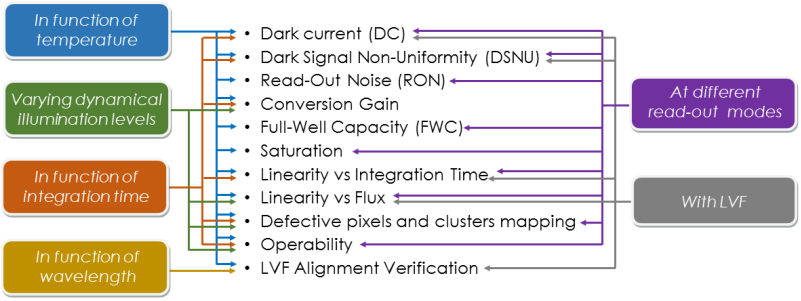

Figure 2. Parameters measured during the characterization of the MAJIS SM VIS-NIR FPU.

In this manuscript, we present the followed methodology to measure each of the parameters of the SM campaign, and a discussion concerning the data analysis performed to derive the key performances of the detector. A comparison with respect to the methodology and results obtained from the FM campaign is also provided. Besides, we describe the design of the VIS-NIR facility used for the MAJIS SM detector characterization campaign, especially the main updates performed after the FM campaign.

2. VIS-NIR CHARACTERIZATION FACILITY

The full characterization of a detector response is possible after performing a wide series of tests. These tests are performed under different illumination conditions (from complete dark to maximum response of the detector), different temperatures (according to the thermal cases at which the detector could be exposed), different wavelengths (including wavelengths slightly outside the spectral sensitive range), different integration times, and the different electronic configurations of the detector when reading-out the generated signal. These tests can only be possible through a highly versatile facility.

The facility developed for the characterization of the MAJIS VIS-NIR detectors is well described in Bolsée et al., 2020[5] (Fig. 3). A monochromatic and tunable light beam is obtained by combining a 1000 W Tungsten-Halogen Quartz lamp (QTH) and a double monochromator. The stability of the intensity of the lamp is from 0.2 % to 0.3 %, and it is continuously monitored by a multi-channels filter radiometer. PbS and Si photodiodes are used to perform radiance stability monitoring at the monochromator level. A condenser focalizes the light beam into the entrance slit of the monochromator. Up to 30 different illumination levels can be provided thanks to the combination of nine neutral density filters installed in two filter wheels. These filters have different optical densities and were selected in such a way that all cross combinations of filters contribute to a uniform sampling of the illumination level, from the maximum flux to a flux lowered by four orders of magnitude. Moreover, a slight wavelength change can offer a new set of 30 slightly different illumination levels due to the spectral distribution of the QTH lamp combined to the spectrometer and optical fiber transmissions.

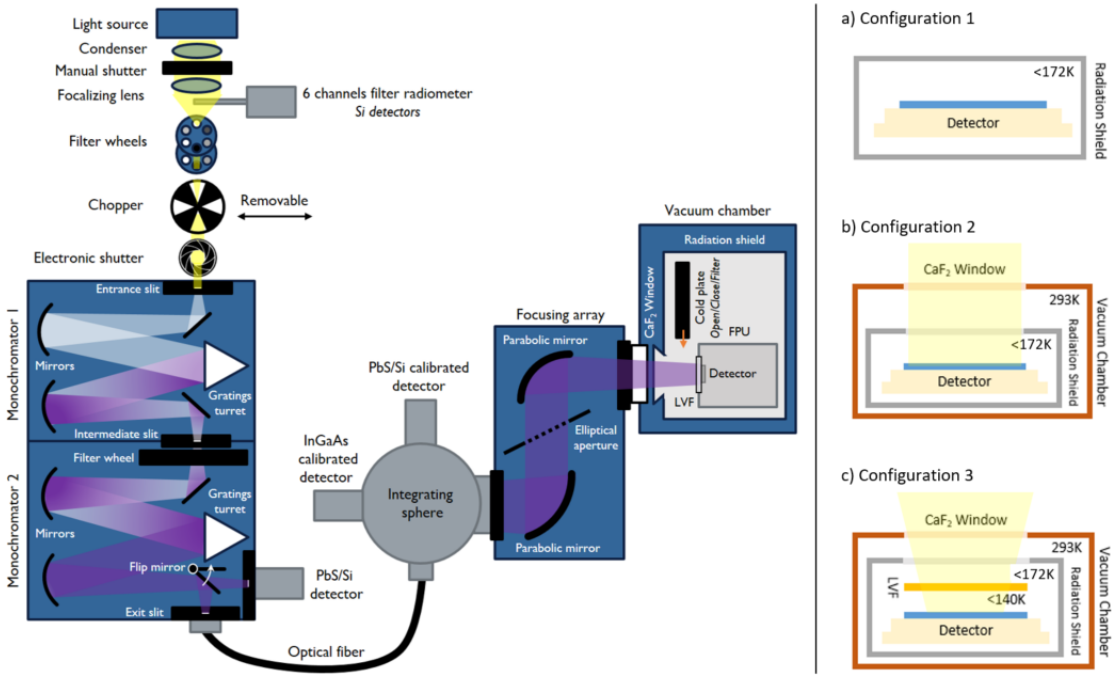

Figure 3. Optical diagram of the VIS-NIR characterization facility. In configuration 1 (a), the facility provides dark conditions by closing the cold plate inside the radiation shield. In configuration 2 (b), the output of the integrating sphere is directly connected to the viewport of the vacuum chamber to provide a uniform light beam to the detector. In configuration 3 (c), the facility reproduces the MAJIS collimating optics.[3]

Consequently, the facility can provide a quasi-infinite levels of illumination. In front of the entrance slit, there is an electronic shutter with a closing time of 40 ms, that allows latency measurements of the detector. However, the electronic shutter was not used during the MAJIS SM characterization campaign. There is also a chopper in the entrance optical path, used for light modulation when a PbS photodiode is installed to monitor the light stability. Thanks to the double monochromator, a high spectral purity with straylight rejection of about 10^{-8}, can be provided by the characterization facility.

On the other hand, high homogeneity of the monochromatic radiance from the monochromator is produced by an Integrating Sphere (IS), which provides enough photon flux for the characterization despite the attenuation induced by the optical fiber that transfers the light from the monochromator to the IS. Two ports of the IS are used by a set of calibrated VIS-NIR photodiodes (PbS and Si) to perform radiance stability monitoring, as well as relative and absolute radiometry when necessary.

The MAJIS SM FPU is thermalized inside a vacuum chamber by the use of a closed cycle cryostat. For the SM characterization campaign, the FPU was thermalized at six different temperatures between 122 K to 145 K with a thermal stability within ± 0.5 K. The vacuum level inside the chamber was generally in the order of 10^{-6} mbar. A detailed description of the cryogenic system can be consulted in Cisneros et al., 2020.[6] However, it is worth to mention that the facility provides a high-security system with redundant thermal control loops, alarms that drive the connection or disconnection of actuators able to keep the FPU (or any other sensitive device inside the vacuum chamber) in safe conditions in case of an undesired event, continuous vacuum and temperature monitoring in real time (even if the measurements campaign is in stand-by), and a user-friendly interface to communicate the status of the detector and the cryogenic system to the operators via email and SMS. This security system was approved by the *Centre National d'Etudes Spatiales* (CNES) and the Belgian User Support and Operations Center (B.USOC) during the different characterization campaigns.[3]

Inside the vacuum chamber, the FPU is surrounded by a cold radiation shield that limits the thermal contribution and straylight from warm objects around the FPU (Fig. 3a). Besides, it includes a movable cold plate with three possible positions: close, open and filter. In the filter position, a customized Short Wave Pass Filter (SWPF) is able to remove the thermal emission of the viewport of the vacuum chamber and other optical items in front of the viewport, between 1.5 μm and 2.65 μm, reducing the undesired straylight on the MAJIS VIS-NIR detector to 10 e^-/pix.[5]

Depending on the measurement to be performed, the facility can be configured in three different ways to provide different illumination conditions to the detector: (1) dark conditions over the MAJIS VIS-NIR operating range, (2) uniform light conditions by installing the IS directly in front of the viewport of the vacuum chamber, and (3) light beam convergence conditions by installing a focusing array between the IS and the viewport of the vacuum chamber, that simulates the convergent beam that the detector will receive after its integration in the MAJIS spectrometer. If necessary for configurations 2 and 3, the movable cold plate could be set to open or filter position.

It is worth to mention that the facility also guarantees ISO-5 cleanliness level. Moreover, the equipment can be remotely controlled and monitored from an ISO-7 area contiguous to the cleanroom. Environmental parameters such as the pressure, oxygen concentration, ambient temperature and relative humidity are continuously monitored. The VIS-NIR characterization facility was developed in 2019 and fully validated in 2020 for its use in space detectors. It is currently available for projects where relative and/or absolute radiometry, as well as cryogenic operating conditions, are required.

3. CHARACTERIZATION CAMPAIGN AND IMPROVEMENTS

The characterization of the MAJIS VIS-NIR SM detector took place in May 2021, by performing the measurements listed in Fig. 2, including the verification of the alignment of the LVF with respect to the FPA. The integration and optical alignment of the FPU in the characterization facility was identical to the procedure followed for the FM campaign.[3] It took place in the ISO-5 area previously described, with a controlled environment in terms of temperature (22 ± 3 °C), relative humidity (45 % - 65 %) and pressure (900 mbar - 1080 mbar). A visual inspection of the status of the FPU, followed by some functional tests before the integration, was performed

at room conditions. Contrarily to the FM characterization campaign, the SM detector was only characterized in its final configuration, i.e., with the LVF installed in front of the FPA.

The FM characterization campaign was performed in June 2020 and it was considered compliant with the defined criteria of success.[3] However, it was limited by the presence of straylight, especially for measurements in dark conditions. For the SM characterization campaign, the design of the radiation shield was slightly improved to avoid straylight from the slit of the movable cold plate (Fig. 4). Following the modifications, the temperature of the radiation shield was decreased by ∼3 K from temperatures reached during the FM characterization campaign with the LVF, and the level of straylight was greatly reduced.

Similarly to the FM characterization campaign,[3] a pre-campaign of measurements was perform to adjust parameters for the proper thermal control of the FPU, to adjust the bias level for frame acquisition, to estimate the straylight present in the detector, and adjust the fluxes and integration times to be used during the measurements. Additionally, a quasi-real-time data processing was performed during the campaign of measurements to verify if criteria of success were met for each parameter.

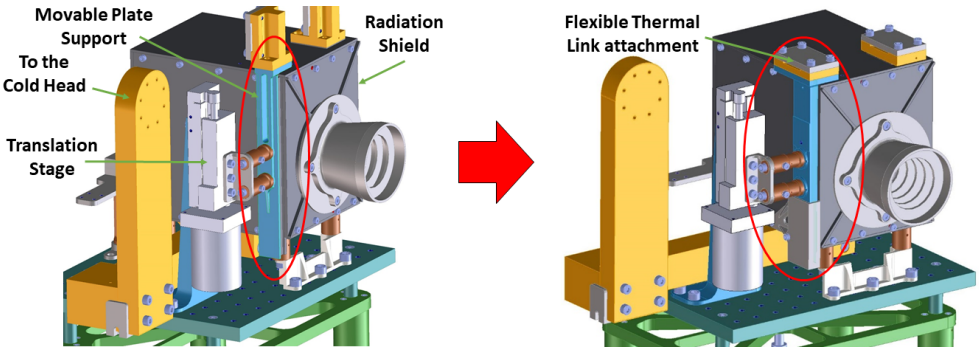

Figure 4. Comparison between the radiation shield used during the characterization campaign of the MAJIS VIS-NIR FM FPU (left) and the updated version used for the SM campaign (right). The improvement reduces the possible straylight from the slit of the movable cold plate inside the radiation shield, where the FPU is installed. An additional shielding piece was added in the low part of the movable piece. The flexible thermal link used to thermalize the movable plate at any position was also modified.

4. MEASUREMENTS AND DATA OVERVIEW

The data from the H1RG SM detector array were all acquired in Correlated Double Sampling (CDS) acquisition mode. In this mode, two successive images are acquired: (1) *reset-read* image, read immediately after the reset switch and (2) *read* image, read after the image defined integration time. The CDS images that result from subtracting *read* and *reset-read* images, are the ones used in the data treatment. The purpose of using a CDS acquisition mode is to remove reset noise, also called kTC noise, which has its origin in the pixel to pixel fluctuations on the reset voltage level of the capacitance nodes prior to the opening of the reset switch.[7]

H1RG detectors have eight reference columns and eight reference rows located at the edges of the detector array , that are not sensitive to light. However, the pixels from the eight reference rows carry the signature of a non-complete removal of the kTC noise, which becomes mostly visible in the eight reference columns. CDS images must be corrected for this residual reset noise effect before further analysis. The details of these corrections are fully detailed in Haffoud, 2020.[8]

The datasets used during the data treatment and data analysis of the SM characterization campaign, are the linearity as a function of integration time, $Lin(DIT)$. A $Lin(DIT)$ dataset consists of nominally $N = 32$ images per integration time, k. The signal for a given (i, j) pixel, $S_{i,j}$, is indexed as $S_{k,n,i,j}$. S is a generic signal measured in dark (Configuration 1), illuminated (Configuration 2/3-OPEN) or background (Configuration 2/3-CLOSED) conditions. $Lin(DIT)$ measurements were performed at Confiuration 2-OPEN at the wavelength 1352nm. The 1352nm wavelength was chosen, by optimization of the following criteria: 1) maximizing the FPA illuminated surface; 2) choice of a transmission plateau of the SWPF filter, for which the cut-off wavelength is

$1.5\mu m$; 3) a flux level allowing to adequately cover the full FPA dynamic range. At this wavelength, the LVF is opaque for approximately one third of the detector surface.

The following quantities, derived from the $Lin(DIT)$, will be used recurrently during this section. For the sake of clearness, all the defined quantities are given for a specific integration time, and the subscript prefix k will be drooped. $P = 1016$ is the number of usable pixels.

- Pixel temporal noise: $\sigma_{i,j} = std\left(S_{i,j,n=1:N}\right)$ (1)
- Mean frame: $\overline{S_{i,j}} = mean\left(S_{i,j,n=1:N}\right)$ (2)
- Median signal of the mean frame: $\widetilde{S} = median\left(\overline{S_{i,j}}\ _{i,j=1:P}\right)$ (3)
- Median noise of the mean frame: $\widetilde{\sigma} = median\left(\overline{\sigma_{i,j}}\ _{i,j=1:P}\right)$ (4)

4.1 LVF alignment

The SM LVF was installed and aligned at IAS prior to the SM characterization campaign. Its alignment with respect to the SM FPA was measured using a microscope. A complementary LVF alignment measurement was performed at BIRA-IASB during the SM characterization campaign. Figure 5 shows a fully illuminated detector, where the LVF fiducial marks are clearly visible. The deviation from the nominal distances from the center of the fiducial marks to the center of the FPA, pixel $(511.5, 511.5)$, measured from the image were used to derive the LVF-FPA alignment accuracy. These deviations were of 2.5 pixels (45 μm) and 1.5 pixels (27 μm) for Y-direction and X-direction, respectively. These measurements are in agreement with IAS microscopic measurements within a maximum deviation of 3 pixels (45 μm).

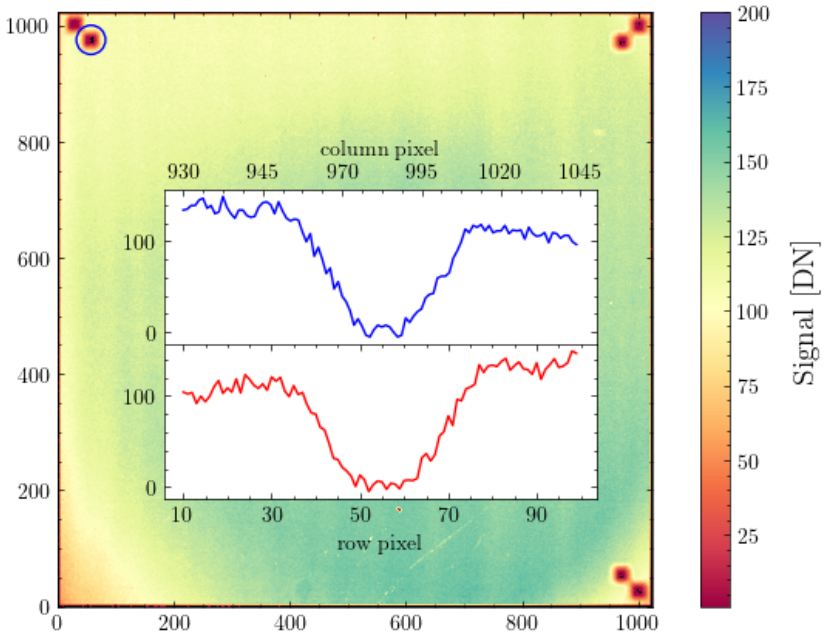

Figure 5. Image acquired at 1800 nm, at 1MHz and 50ms integration time, in Configuration 3. The 6 fiducials marks used to measure the LVF alignment with respect to the FPA are clearly visible. The row and column pixel profiles of the lower fiducial mark from the top left corner are shown in the inset plot.

4.2 Dark current

The Dark Current (DC) rate of the detector was measured with the optical bench in Configuration 1, for a range of FPA temperatures varying from 122 K to 145 K. For each temperature, the DC value in Digital Number per second $DN \cdot s^{-1}$, was derived from the peak of the histogram,[8] for all the pixels of a dark $Lin(DIT)$ measurement, as shown in Fig. 6. The DC values for both readout modes of the detector (100 kHz and 1 MHz), and for each temperature at which both were measured, are shown in Tab. 1.

Table 1. DC rate in $DN \cdot s^{-1}$ units, for the complete range of FPA temperatures.

	122 K	126 K	129 K	137 K	141 K	145 K
100 kHz	4.9	10.3	16.9	79.3	166.0	366.8
1 MHz	0.29	0.98	1.4	5.9	12.5	24.4

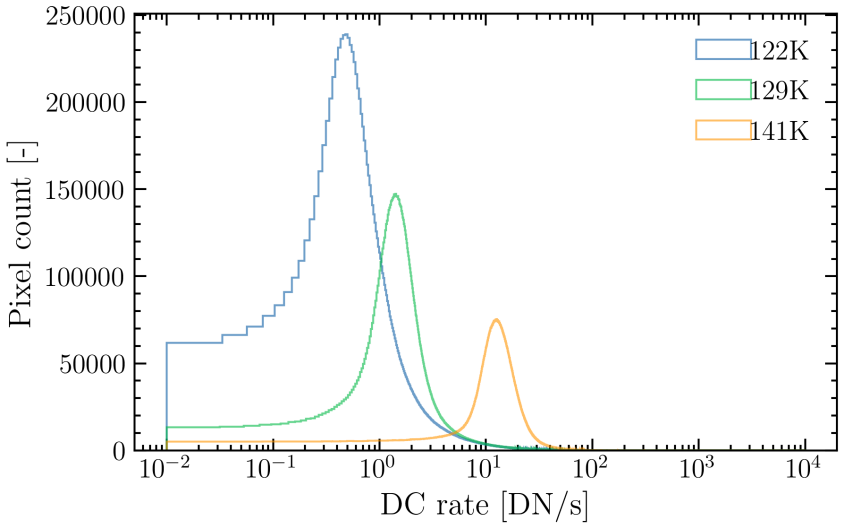

Figure 6. DC rate distribution for three of the FPA operating temperatures.

4.3 Read Out noise

The Read Out Noise (RON) is a signal-independent noise that includes namely the Dark Signal Non-Uniformity (DSNU), and it is determined from Eq. 5, where $TotalNoise$ is the pixel temporal noise, given by Eq. 1. The DC signal follows the Poisson statistics, so that the associated shot noise is given by the square-root of the DC value per pixel.

$$TotalNoise^2 = ShotNoise^2 + RON^2 \tag{5}$$

Figure 7 shows the RON mapping derived from Eq. 5 with the corresponding histograms of the RON and Total noise of the SM detector. The RON values found with the described method were 1.06 DN and 11.47 DN, for the 1 MHz and 100 kHz read-out modes, respectively, for a FPA temperature of 129 K. No RON temperature dependence was detected.

4.4 Linearity

The objective of the analysis of the linearity measurement is to quantify the capacity of a given detector in delivering a readout signal proportional to the signal received by the detector. This analysis can be performed by

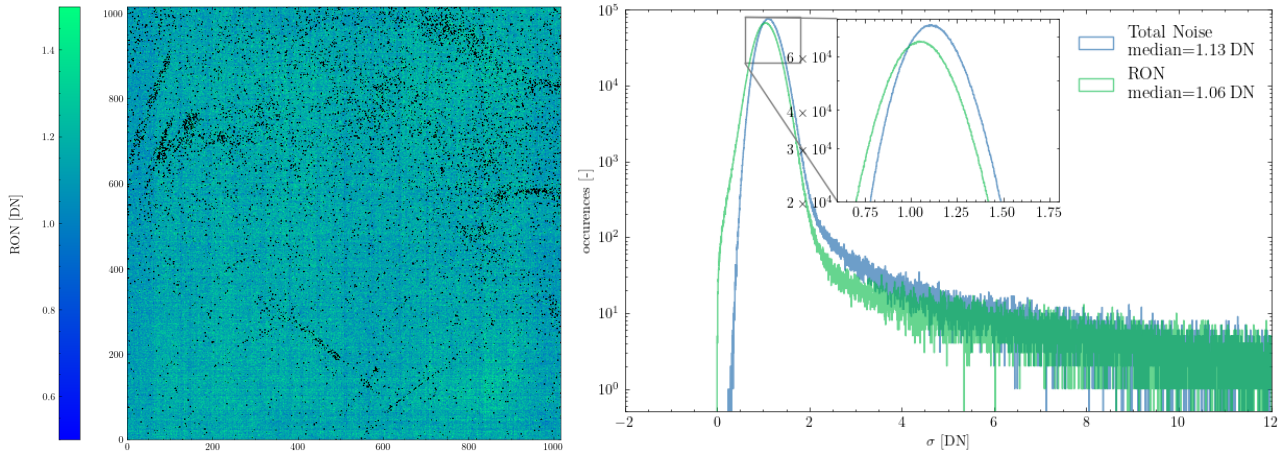

Figure 7. Left panel: Mapping of the RON with SM FPA at 129 K, 1 MHz readout mode and 4000 ms of integration time; the out of scale RON values are represented by the black colour. Right panel: Depiction of the application of Eq. 5 to determine the RON of the SM detector.

modulating the signal received by the detector, while keeping the detector integration time constant, $Lin(Flux)$, or by varying the detector integration time for a constant input signal, $Lin(DIT)$. This last measurement type is analyzed in this section. From the linearity analysis, important detector parameters such as the quantification of the detector non-linearity and the Full-Well Capacity (FWC) can be derived.

Figure 8 depicts the non-linearity present in H1RG detectors: by assuming a perfectly linear relation between the integration time and the readout signal for data points well below saturation regime, the response of a perfect detector can be simulated and compared to the one of the real detector.

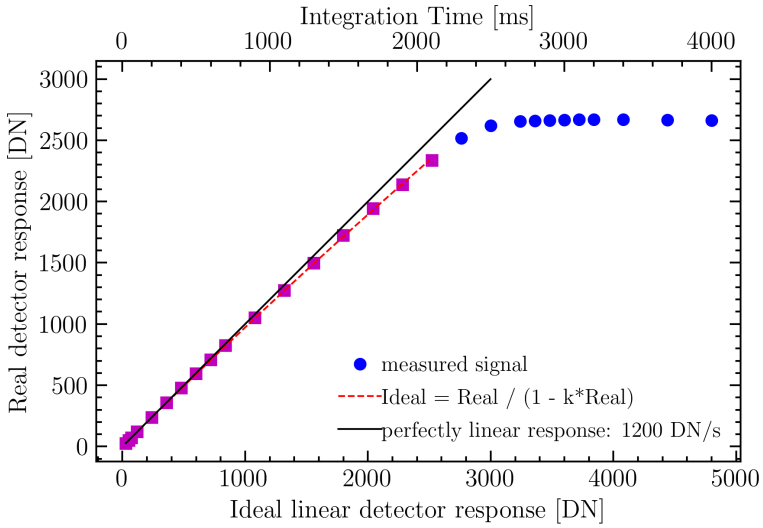

Figure 8. MAJIS SM FPA linearity at 1 MHz readout mode and 129K FPA temperature, as a function of both integration time (top xx axis) and ideal detector response (bottom xx axis). The ideal detector response is plotted in black (1200 DN/s), and deviation from the real detector is noticeable as from 1500 DN or 1000 ms. A relation between a perfectly linear detector and a real detector is expressed in Eq. 6, fitted by using the data represented by the magenta squares in this plot.

The H1RG non-linearity shown in Fig. 8 is due to the decrease of the transimpedance of the sensing node with the increase of the collected charge, represented by k in Eq. 6. I and R, refer to the signals measured by a

perfectly linear and real detectors, respectively. Fitting Eq. 6, yields $k = 2.45 \times 10^{-5}\ DN^{-1}$.

$$I = \frac{R}{1 - k.R} \tag{6}$$

The signal corrected for the decrease of transimpedance of the sensing node I, according to Eq. 6, is shown in Fig. 9 as a function of the integration time. The deviation to linearity, defined as the percentual difference between I and the linearity, is also plotted in Fig. 9.

The linear range value, defined as the corrected signal at which it deviates 5% from the linearity,[4] shown in Fig. 9 is of 2566 DN.

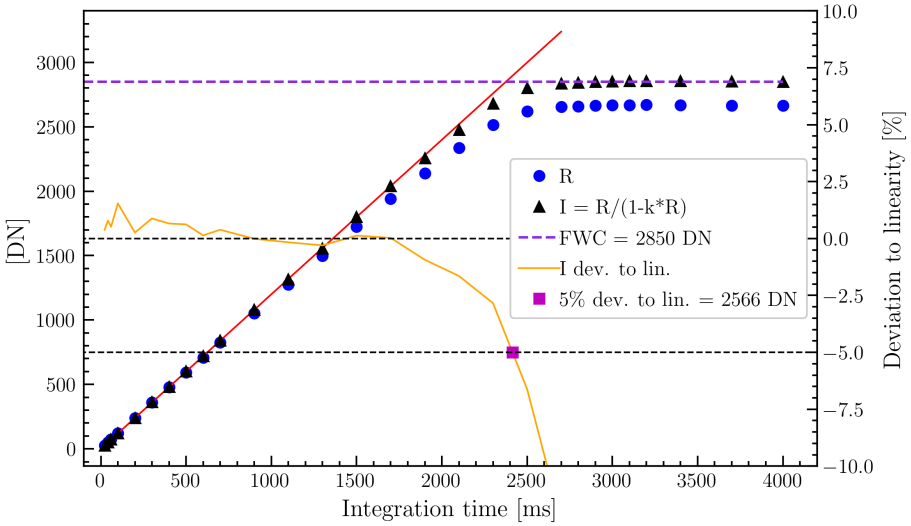

Figure 9. Comparison between signal from an ideal detector (red line), the actual measured signal, R, and the measured signal corrected for transimpedance, I, according to Eq. 6, for 1MHz readout mode and 129K FPA temperature. The FWC is defined as the asymptotic signal level on the saturation regime and equals 2850 DN. The 5% deviation of the corrected signal, marks the end of the non-linearity regime of the detector,[4] at 2566 DN.

4.5 Conversion gain

In order to attribute a measurable physical quantity to the detector parameters, the conversion gain, G, must be calculated. It is defined as the number of electrons needed to generate one digital unit, and is given in $e^- \cdot DN^{-1}$.

The calculation of the gain follows the mean shot-variance method,[9] with Eq. 7 stating the noise components present in the illuminated frames.

$$Total^2_{Noise} = RON^2 + Shot^2_{Noise} + Spatial^2_{Noise} \tag{7}$$

For a given integration time, the total noise is calculated as in Eq. 4. The spatial noise is determined by noise subtraction of consecutive frames,[9] with the RON being determined in Section 4.3.

The mean shot-variance method to determine the conversion gain is shown in Fig. 10, based on Eq. 8, where $Signal$ is determined according to Eq. 3 and corrected for the transimpedance factor k, according to Eq. 6.

$$Shot^2_{Noise} = Signal \frac{1}{Gain} \tag{8}$$

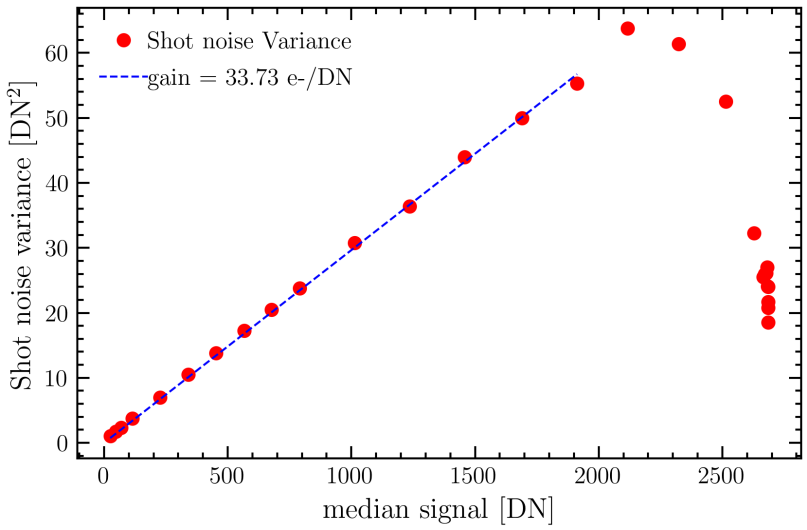

Figure 10. Depiction of the mean shot-variance, for SM detector readout at 1 MHz with a temperature of 129 K. The method to determine the detector conversion gain, is given by the reciprocal of the slope, according to Eq. 8.

4.6 Operability

The operability of the detector quantifies the amount of usable pixels, which is reduced from the original 1016×1016 matrix (without the reference pixels), due to the presence of three types of non-operational pixels: warm, hot and dead.

4.6.1 Warm Pixels

Warm pixels are defined as having a RON higher than 70 e^- (Section 4.3). The occurrence of warm pixels increases with temperature and integration time. Figure 11 illustrates this increase observed when characterizing the FPA at 129 K with integration times of 600 ms and 4000 ms.

As observed in Fig. 11, warm pixels tend to distribute around large clusters, specially visible for larger integration times. With the SM FPA thermalized at 129 K, and readout at 1 MHz with 4000 ms of integration time, the total number of warm pixels amounts to $\sim 7.7 \times 10^3$, representing a 0.75% fraction of the FPA total usable pixel area of 1016×1016 pixels. This represents roughly three times the amount of warm pixels for an integration time of a 600 ms.

The patterns of warm pixels clusters are easily identified for longer integration times. Some of the thinner linear structures, in the lower center and top left corner of the sensitive area of the SM detector, for instance, are partly visible for the 600 ms integration time.

4.6.2 Dead Pixels

Dead pixels are defined as pixels having a CDS signal lower than 200 e^-, for frames where the median frame value is at least half of the FWC, roughly 48 ke^- and 46 ke^- for the 1 MHz and 100 kHz readout modes, respectively. Similarly to the warm pixels, which tend to group around clusters, dead pixels group around smaller and more isolated clusters, as shown in Fig. 12.

The dead pixels count estimation should ideally be performed using a fully illuminated FPA. For this, a dataset of images acquired at 2350 nm were analyzed as shown in Fig. 12. Approximately 90 dead pixels were found in this image. At this wavelength, due to the low available signal and lower detection efficiency, the median signal of these images is around 33 ke^- and thus does not comply with the condition of a median signal higher than 50% of the FWC (~ 48 ke^-). To overcome this limitation, another dataset of images, acquired at 1352 nm was used. At this wavelength, roughly the left third of the detector falls on the LVF cut-off region, meaning this

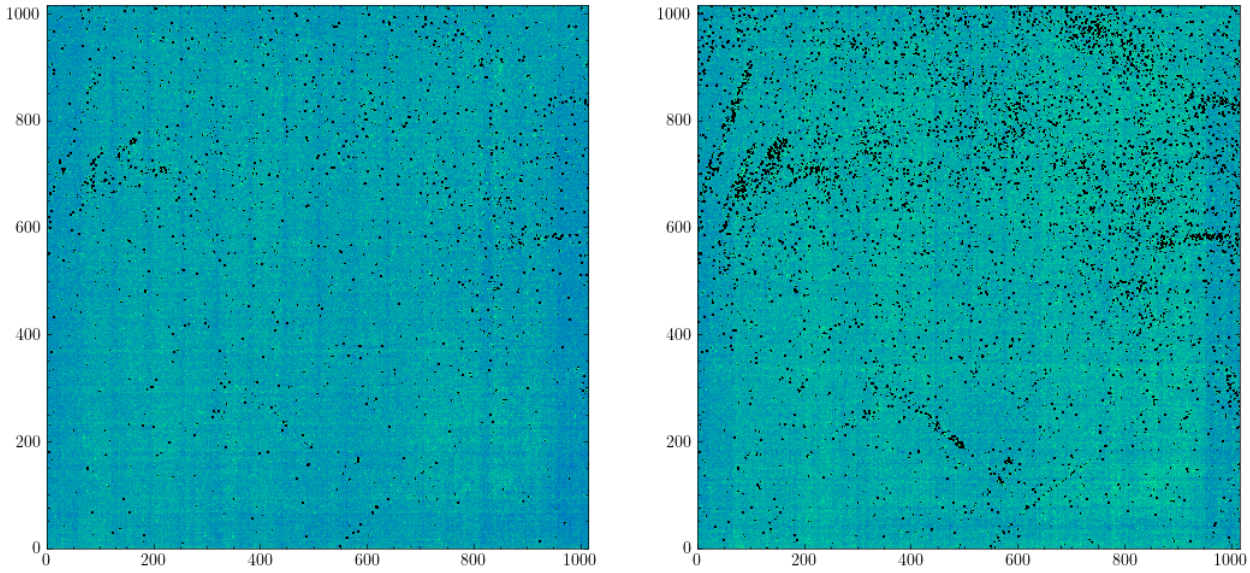

Figure 11. RON map of the SM detector, with the identification of warm pixels in black, for 132 K at 1 MHz. Left panel: 3136 warm pixels identified with 600 ms of integration time. Right panel: 7664 warm pixels identified with 4000 ms of integration time.

pixel fraction could not be evaluated for dead pixels as its signal is nominally zero. The analysis of this dataset could lead to a slight overestimation of the number of 90 dead pixels, as clarified below.

The dead pixel count of cluster D2 (Fig. 12, right panel, top right plot) was analyzed for nominal linearity measurements (at 1352 nm), where a whole range of median images signals is available. The number of dead pixels in cluster D2 is consistent for a median signal of 32 ke^-, and it sensibly but steadily decreases to 24 dead pixels for median signals verifying the condition of FWC $> 50\%$. This dynamic outside the clusters might be different, but an estimation of 70-80 dead pixels (less than 0.01% of the total usable pixel area), is a reasonable approximation.

The above reasoning is transferable to other FPA operating temperatures and readout modes. Although no significant dependence was observed in the amount of dead pixels between both readout modes, a slight temperature dependence was found: 70, 90 and 110 dead pixels for FPA at temperatures of 122K, 129K and 141K.

4.6.3 Hot Pixels

Hot pixels are defined as pixels presenting a signal in excess of 200% of the image median signal, for images where the median signal is less than 10% of the FWC, corresponding to approximatelly 9 ke^-. Contrary to the dead pixels estimation, a partially *covered* detector, due to LVF cut-off, allows to determine the quantity of hot pixels, due to the fact that their signal is independent of the received flux. Unlike dead and warm pixels, hot pixels are isolated, with no grouping on clusters.

As in for the dead pixels, no dependence on the readout mode was found. However, the temperature dependence is significant, with 80, 150 and 600 hot pixels for FPA temperatures of 122K, 129K and 141K, respectively.

5. CONCLUSIONS

The cryogenic and radiometric capabilities of the VIS-NIR characterization facility allowed to successfully complete the MAJIS SM FPA characterization plan measurements. This facility was also used to characterize the MAJIS FM detector,[3] although it was improved, in between both campaigns, to reduce the amount of straylight present during the SM measurements.

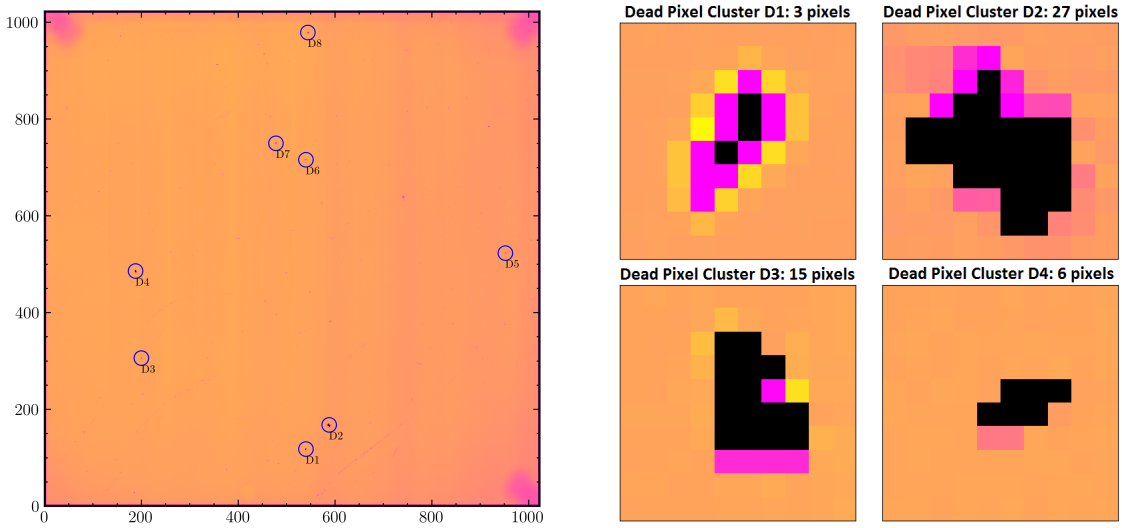

Figure 12. Dead pixels mapping for $21ke^-$ ($\sim$ 37% of FWC). Left panel: Full map of dead pixels with identification of the eight main clusters found. Right panel: Detail of clusters 1, 2, and 4.

In the radiometric plan, the light source stability and respective radiometric monitoring were key to perform long duration linearity measurements, extensively used in the detector performance calculation.

The main detector parameters derived in this work are presented in Tab. 2 for both readout modes of the detector, 100 kHz and 1 MHz.

The comparison between MAJIS VIS-NIR FM and SM FPA parameters[10,11] is excellent for the gain, with less than 1% difference for both modes. The SM RON value is very similar to the FM (34 e^-) for the 1MHz mode, but much less so for the 100kHz mode where the SM RON is roughly 30% higher than that of the FM (19 e^-). There is a substantial difference for the FWC at 1MHz, with the SM FWC being lower by $\sim$ 9 $ke-$; this difference is less pronounced for the 100kHz mode, with a $\sim$ 3 $ke-$ deficit for the SM. These deviations reflect the inherent differences between both detectors, and might partially reflect accessory differences in data processing and analysis.

Table 2. MAJIS VIS NIR SM detector performance parameters for a 129K FPA temperature

	FWC $[ke^-]$	**k** $[DN^{-1}]$	**RON** $[e^-]$	**Gain** $[e^-/DN]$
100k Hz	96	1.71×10^{-6}	25	2.18
1 MHz	92	2.45×10^{-5}	36	33.73

ACKNOWLEDGMENTS

This project acknowledges funding, (i) by the Belgian Science Policy Office (BELSPO) by PRODEX-11 Project Proposal: *Characterization of JUICE/MAJIS VIS-NIR detectors* (PEA 4000124255); (ii) by the ESA JUICE Project; and (iii) by the Scientific Research Fund (FNRS) by the Aspirant Grant: 34828772 *MAJIS detectors and impact on science.*

REFERENCES

[1] Grasset, O. et al., "JUpiter ICy moons Explorer (JUICE): An ESA mission to orbit Ganymede and to characterise the Jupiter system," *Planetary and Space Science* **78**, 1–21 (2013).

[2] Piccioni, G. et al., "Scientific goals and technical challenges of the MAJIS imaging spectrometer for the JUICE mission," in [*5th International Workshop on Metrology for AeroSpace (MetroAeroSpace)*], 318–323, IEEE (2019).
[3] Cisneros-González, M. E. et al., "MAJIS/JUICE VIS-NIR FM and SM detectors characterization," in [*Space Telescopes and Instrumentation: Optical, Infrared, and Millimeter Waves*], *Proc. SPIE* **11443**, 271–285 (2020).
[4] MAJIS Team, "MAJIS FPU VIS-NIR Requirement Specifications," tech. rep., Institut d'Astrophysique Spatiale (IAS) (2018). Ref: JUI-IAS-MAJ-RS-021.
[5] Bolsée, D. et al., "Characterization facility for the MAJIS/JUICE VIS-NIR FM and SM detectors," in [*Space Telescopes and Instrumentation: Optical, Infrared, and Millimeter Waves*], *Proc. SPIE* **11443**, 1214–1233 (2020).
[6] Cisneros-González, M. E. et al., "The thermal-vacuum and security system of the characterization facility for MAJIS/JUICE VIS-NIR FM and SM detectors," in [*Space Telescopes and Instrumentation: Optical, Infrared, and Millimeter Waves*], *Proc. SPIE* **11443** (2020).
[7] James, W. Beletic et al., "Teledyne Imaging Sensors: infrared imaging technologies for astronomy and civil space," in [*High Energy, Optical, and Infrared Detectors for Astronomy III*], *Proc. SPIE* **70210** (2008).
[8] Haffoud, P., *MAJIS instrument characterization*, Master's thesis, Delft University of Technology, Delft, Netherlands (2020).
[9] Janesick, J. R., [*Photon Transfer*], SPIE Press (2007).
[10] Haffoud, P. et al., "MAJIS Focal Plane Unit: 2) Performances of the VI channel," *Proc. SPIE* **This conference** (2022).
[11] Langevin, Y. et al., "H1RG readout procedures for MAJIS, the VISNIR-IR imaging spectrometer of JUICE," *Proc. SPIE* **This conference** (2022).

APPENDIX A. ACRONYMS

ASIC	Application-Specific Integrated Circuit
BELSPO	Belgian Science Policy Office
BIRA-IASB	Royal Belgian Institute for Space Aeronomy
BUSOC	Belgian User Support and Operations Center
CDS	Correlated Double Sampling
CNES	Centre National d'Etudes Spatiales
DC	Dark Current
DIT	Detector Integration Time
DN	Digital Number
DSNU	Dark Signal Non-Uniformity
ESA	European Space Agency
FM	Flight Model
FNRS	Scientific Research Fund
FPA	Focal Plane Array
FPAssy	Focal Plane Assembly
FPE	Focal Plane Electronics
FPF	Focal Plane Flex
FPU	Focal Plane Unit
FWC	Full-Well Capacity
IAS	Institute of Space Astrophysics

IR	InfraRed wavelength range
IS	Integrating Sphere
ISO	International Organization for Standardization
JUICE	JUpiter Icy Moons Explorer
LVF	Linear Variable Filter
MAJIS	Moons And Jupiter Imaging Spectrometer
NIR	Near-InfraRed wavelength range
OH	Optical Head
QTH	Quartz Tungsten Halogen
ROB	Royal Observatory of Belgium
RON	Read-Out Noise
SIDECAR	System Image, Digitizing, Enhancing, Controlling, And Retrieving
SM	Spare Model
SWPF	Short Wave Pass Filter
VIS	VISible wavelength range